

Photometry of the Four Anti-Galactocentric Old Open Clusters: Czernik 30, Berkeley 34, Berkeley 75, and Berkeley 76

HYOBIN IM,^{1,2} SANG CHUL KIM,^{1,2,3,*} JAEMANN KYEONG,¹ HONG SOO PARK,^{1,2,3} AND JOON HYEOP LEE¹

¹*Korea Astronomy Space Science Institute (KASI), 776 Daedukdae-ro, Yuseong-gu, Daejeon 34055, Republic of Korea*

²*Korea University of Science and Technology (UST), 217 Gajeong-ro, Yuseong-gu, Daejeon 34113, Republic of Korea*

³*Visiting astronomer, Cerro Tololo Inter-American Observatory at NSF's NOIRLab, which is managed by the Association of Universities for Research in Astronomy (AURA) under a cooperative agreement with the National Science Foundation.*

ABSTRACT

We present a *BVI* photometric study of four old open clusters (OCs) in the Milky Way Galaxy, Czernik 30, Berkeley 34, Berkeley 75, and Berkeley 76 using the observation data obtained with the SMARTS 1.0 m telescope at the CTIO, Chile. These four OCs are located at the anti-Galactocentric direction and in the Galactic plane. We determine the fundamental physical parameters for the four OCs, such as age, metallicity, distance modulus, and color excess, using red clump and PARSEC isochrone fitting methods after finding center and size of the four OCs. These four old OCs are 2 – 3 Gyr old and 6 – 8 kpc away from the Sun. The metallicity ([Fe/H]) values of the four OCs are between –0.6 and 0.0 dex. We combine data for these four OCs with those for old OCs from five literatures resulting in 236 objects to investigate Galactic radial metallicity distribution. The gradient of a single linear fit for this Galactocentric [Fe/H] distribution is -0.052 ± 0.004 dex kpc^{–1}. If we assume the existence of a discontinuity in this radial metallicity distribution, the gradient at Galactocentric radius < 12 kpc is -0.070 ± 0.006 dex kpc^{–1}, while that at the outer part is -0.016 ± 0.010 which is flatter than that of the inner part. Although there are not many sample clusters at the outer part, the broken linear fit seems to better follow the observation data.

Keywords: Open star clusters (1160); Red giant clump (1370); Galaxy disks (589); Galaxy evolution (594); Galaxy abundances (574); Milky Way evolution (1052); Chemical abundances (224)

1. INTRODUCTION

Most stars in the Milky Way Galaxy (MWG) are born in star clusters (Lada & Lada 2003; Kim et al. 2009; Kyeong et al. 2011). The stars in open clusters (OCs) share some physical values, such as distance, age, and chemical composition, which can be determined using photometric methods (Park & Lee 1999; Kyeong et al. 2001, 2008; Ahumada et al. 2013; Carrera et al. 2017). OCs can be divided into three groups by age: old OCs have ages older than 1 Gyr, young OCs have ages younger than 1 Myr, and intermediate-age OCs have ages of 1 Myr – 1 Gyr (Friel 1995). Young OCs are useful for investigating star formation processes, while old OCs are a good tool for research on the formation and early evolution of the Galactic disk and examination of stellar evolution models (van den Bergh & McClure 1980; Lada & Lada 2003).

There are many Galactic OC catalogs. Lyngå published ‘Catalog of Open Cluster Data’ that includes 1148 OCs with physical parameters, like diameter, age, metallicity, and reddening (Lyngå 1995). Dias et al. (2002) catalog of version 3.5 includes 2167 MWG OCs with the information about location, kinematics, distance, age, and reddening. The Milky Way Star Cluster catalog of Kharchenko et al. (2013) increased the number of OCs to 2808.

The number of OCs in catalogs goes up, but the number of OCs with known physical parameters are much less than the total number of OCs in the catalogs. Since the beginning of the *Gaia* era, many studies have estimated parameters such as distance and age with *Gaia*. Using the *Gaia* DR2 data, Cantat-Gaudin et al. (2018a) published a list of 1229 OCs including physical parameters like age, distance, proper motion, and parallax. Liu & Pang (2019) included 2443 cluster candidates with parameters from isochrone fitting. Using *Gaia* DR2 data, the Gaussian mixture model, mean-shift algorithms and

* Corresponding author.

visual inspections, [Sim et al. \(2019\)](#) discovered 207 new OCs. Although OC catalogs are being updated, there are disagreements about the physical parameters of the same object among the studies in the catalogs. [Cantat-Gaudin et al. \(2020\)](#) used machine learning method to fit isochrone models to the *Gaia* DR2 data and obtained parameters (age, distance, and extinction) for 2000 OCs. [Dias et al. \(2021\)](#) provided physical parameters, such as proper motion, radial velocity, distance, age, and $[\text{Fe}/\text{H}]$, for 1743 OCs based on the *Gaia* DR2 data.

The old OCs with larger Galactocentric distances are important for studying metallicity distribution in the Galactic disk. [Janes \(1979\)](#) found the Galactic disk metallicity gradient using OCs. [Twarog et al. \(1997\)](#) argued the existence of a discontinuity in radial metallicity distribution outside of 10 kpc from the Galactic center, where the inner part shows a steeper gradient than the outer part. The position of the discontinuity is suggested to be at 10 – 15 kpc in recent studies ([Netopil et al. 2016](#); [Kim et al. 2017](#); [Donor et al. 2020](#); [Monteiro et al. 2021](#)). However, the number of well-studied OCs at the outer part of the Galactic disk is currently too small to clearly determine the existence and position of the discontinuity.

One of the strengths of studying the anti-Galactocentric region is the relatively lower extinction, which enables us to investigate the evolution of the outer part of the Galactic disk. The old OCs in the anti-Galactocentric region can be a useful tool for studying the evolution of the MWG since they hold a long dynamic timescales ([Gaia Collaboration et al. 2021](#)).

We investigated the physical parameters of four OCs located in the anti-Galactocentric direction: Czernik 30, Berkeley 34, Berkeley 75 and Berkeley 76 by using the red clump (RC) stars and by fitting the PAdova and TRieste Stellar Evolution Code (PARSEC) isochrones ([Bressan et al. 2012](#)).

In Table 1, we summarize the physical parameters of the four OCs obtained by the previous studies and in our study. Czernik 30 is located at $\alpha_{J2000} = 07^h31^m10.8^s$ and $\delta_{J2000} = -09^\circ56'42''$ and has been studied in four literatures. [Hasegawa et al. \(2008\)](#) and [Piatti et al. \(2009\)](#) presented physical parameters using *BVI* photometric data and Washington photometric data. [Perren et al. \(2015\)](#) made a code for the automatic determination of physical parameters of OCs, and included Czernik 30 in their sample for testing the code and gave the physical parameters. [Hayes et al. \(2015\)](#) conducted a photometric and spectroscopic study of Czernik 30 and obtained the basic parameters.

The position of Berkeley 34 is $\alpha_{J2000} = 07^h00^m23.2^s$, $\delta_{J2000} = -00^\circ13'54''$ and there are three previous stud-

ies for this cluster. [Hasegawa et al. \(2004\)](#) and [Ortolani et al. \(2005\)](#) presented the physical parameters using isochrone fitting. [Donati et al. \(2012\)](#) presented ranges for the physical parameters and calculated the binary fraction, which is measured from color and magnitude and fine-tuning with differential reddening value.

Berkeley 75 is located at $\alpha_{J2000} = 06^h48^m59.1^s$, $\delta_{J2000} = -23^\circ59'36''$. [Carraro et al. \(2005\)](#) published the physical parameters using the *BVI* photometry and [Carraro et al. \(2007\)](#) studied five OCs at the outer Galactic disk including Berkeley 75 using VLT high resolution spectroscopic data, and suggested the physical parameters. [Cantat-Gaudin et al. \(2016\)](#) studied the abundances and kinematics of ten OCs including Berkeley 75. They used the spectroscopic data of two member stars of Berkeley 75 and gave the $[\text{Fe}/\text{H}]$ value of Berkeley 75.

The location of Berkeley 76 is $\alpha_{J2000} = 07^h06^m42.4^s$, $\delta_{J2000} = -11^\circ43'33''$ and the properties of Berkeley 76 from three previous studies have a relatively wider range. [Hasegawa et al. \(2008\)](#) and [Tadross \(2008\)](#) obtained the physical parameters from isochrone fittings to the *BVI* photometric data and 2MASS *JHK* data. [Carraro et al. \(2013\)](#) studied five old OCs at the outer Galactic disk including Berkeley 76 and they determined the parameters. The distance modulus from [Hasegawa et al. \(2008\)](#) and [Carraro et al. \(2013\)](#) differ by almost 3 magnitudes.

This study uses the observation data obtained from the same observing run as that of [Kim et al. \(2017\)](#), which presented the physical parameters of the old OC Ruprecht 6. To better constrain the evolution of the outer part of the Galactic disk, in this paper, we estimate the physical parameters of the four OCs in a way basically consistent with that of [Kim et al. \(2017\)](#) but more improved. In this study, we use the *Gaia* Early Data Release 3 (EDR3) data to select member stars of the clusters and adopt the number density distribution function of the stellar photometry results, to better estimate the centers and radius of the clusters.

This paper is organized as follows. In Section 2, we explain the observations and data reduction. In Section 3, we describe the results on Czernik 30. Section 3 has five subsections : the center of Czernik 30, radius, member selection using the *Gaia* EDR3 data, reddening and distance, age and metallicity, and comparison with previous studies. In Sections 4, 5, and 6, we show the results for Berkeley 34, Berkeley 75, and Berkeley 76, respectively, using the same routines as in section 3. In Section 7, we show and discuss the radial metallicity distribution of the Galactic disk, using the previously known OCs from the literature and the newly estimated

physical quantities of the four OCs together. In Section 8, we summarize our results.

2. OBSERVATIONS AND DATA REDUCTION

The *BVI* images for the four target OCs, Czernik 30, Berkeley 34, Berkeley 75, and Berkeley 76, were acquired at the Small and Moderate Aperture Research Telescope System (SMARTS) 1.0 m telescope with the Y4KCam camera at the Cerro Tololo Inter-American Observatory (CTIO) in 2010 December. Y4KCam has 4064×4064 pixels and the pixel scale is $0.289'' \text{ pixel}^{-1}$ and the field of view (FoV) is $19.57' \times 19.57'$. While the R.A. and declination are in Table 1, Table 2 lists Galactic longitudes, Galactic latitudes, and the radii of the four OCs. Figure 1 shows the centers and radii of the OCs together with the center positions from previous studies. Table 3 lists the observation log showing the observation date, filter and exposure times.

While the reduction and photometry routines were the same as those applied as in Kim et al. (2017), we summarize the key processes here. IRAF¹/CCDRED package has been used for the standard reduction processes of overscan correction, bias correction, and sky flattening. Point spread function (PSF) photometry has been performed by using the DAOPHOT II/ALLSTAR stand-alone package (Stetson 1990). The error values of the PSF photometry are shown in Fig. 2. To derive the astrometry solution, *astrometry.net* (Lang et al. 2010) has been used.

Four Landolt standard star fields (PG0231+051, LB1735, LSS982, Rubin 149) (Landolt 1992; Landolt & Uomoto 2007; Landolt 2009) were observed to obtain the standardization equations to convert the instrumental magnitudes to standard magnitudes. The same transformation equations as those in Kim et al. (2017) are used, which are

$$\begin{aligned} B &= b - 0.285(\pm 0.009) X_b - 0.127(\pm 0.005)(B - V) - 1.903(\pm 0.013) \\ V &= v - 0.157(\pm 0.007) X_v + 0.027(\pm 0.004)(B - V) - 1.693(\pm 0.011) \\ I &= i - 0.056(\pm 0.007) X_i + 0.019(\pm 0.003)(V - I) - 2.712(\pm 0.010) \end{aligned}$$

where b, v, i are instrumental magnitudes for each band, B, V, I are standard magnitudes, and X means airmass for each band. The rms values of the standardization residuals (standard magnitude minus transformed magnitude) are $\Delta B = 0.037$, $\Delta V = 0.030$, and $\Delta I = 0.029$ mag.

3. CZERNIK 30

3.1. Center

To determine the center of Czernik 30, we fit the Gaussian function on the distribution of the point sources detected with the DAOPHOT II routine in Section 2 and brighter than $V = 20$ mag using the Python *Gaussian.kde* function of *Scipy* package with Scott's rule as bandwidth, which is the optimal bandwidth for a Gaussian kernel to minimize the integral value of the mean squared error. We obtain the probability distribution function (PDF) for the whole image, and the peak of this function is considered to be the center of Czernik 30. This result is shown in Fig. 3. The left color bar in Fig. 3 indicates the number of stars brighter than $V = 20$ mag per arcmin square and the right color bar shows the membership probability of each star (see Section 3.2 below).

The red cross symbol in Fig. 1 (a) is the derived center of Czernik 30 : $\alpha_{J2000} = 07^h 31^m 10.8^s$ and $\delta_{J2000} = -09^\circ 56' 42''$. While the center of Czernik 30 used by Hayes et al. (2015) ($\alpha_{J2000} = 07^h 31^m 11^s$, $\delta_{J2000} = -09^\circ 56' 38''$, green x symbol in Fig. 1 (a)) and that used by Piatti et al. (2009) ($\alpha_{J2000} = 07^h 31^m 10^s$, $\delta_{J2000} = -09^\circ 56' 00''$, magenta x symbol in Fig. 1 (a)) are very close to ours, the centers used by Hasegawa et al. (2008) ($\alpha_{J2000} = 07^h 31^m 18^s$, $\delta_{J2000} = -09^\circ 58' 00''$, yellow x symbol in Fig. 1 (a)) and that used by Perren et al. (2015) ($\alpha_{J2000} = 07^h 31^m 19.2^s$, $\delta_{J2000} = -09^\circ 58' 12''$, cyan x symbol in Fig. 1 (a)) are a bit different from ours.

3.2. Member Selection

pyUPMASK (Pera et al. 2021) is a package to determine members of a star cluster using the method of the 'unsupervised photometric membership assignment in stellar clusters' (UPMASK) algorithm (Krone-Martins & Moitinho 2014). UPMASK initially selected the stellar cluster members using the K-mean clustering method with photometric information. Cantat-Gaudin et al. (2018a,b) and Carrera et al. (2019) found the membership of OCs using UPMASK with proper motion and parallax data from *Gaia*. pyUPMASK is developed in Python and supports the clustering method from the scikit-learn library, while UPMASK is written by R and supports the K-mean clustering method. pyUPMASK is composed of two loops: an outer loop and an inner loop. The outer loop runs the inner loop and calculates the membership probability, and the inner loop identifies and rejects clusters. pyUPMASK measures clustering in three dimensional space, such as proper motion and parallax.

We adopted pyUPMASK to select the members of Czernik 30 with proper motion and parallax data from the *Gaia* EDR3. *Gaia* EDR3 data which cover our image region were matched with our photometric catalog. The stars included in the final catalog for selecting members satisfy two conditions: brighter than $V = 20$ mag and parallax greater than 0. Among a dozen clustering methods we adopted the Gaussian mixture model, which assumes every cluster follows a Gaussian function. Finally, 137 member stars were found to have membership probability larger than 0.70, which was also used in Zhong et al. (2022) as a probability limit for member stars.

¹ IRAF is distributed by the National Optical Astronomy Observatories, which is operated by the Association of Universities for Research in Astronomy, Inc. (AURA) under a cooperative agreement with the National Science Foundation.

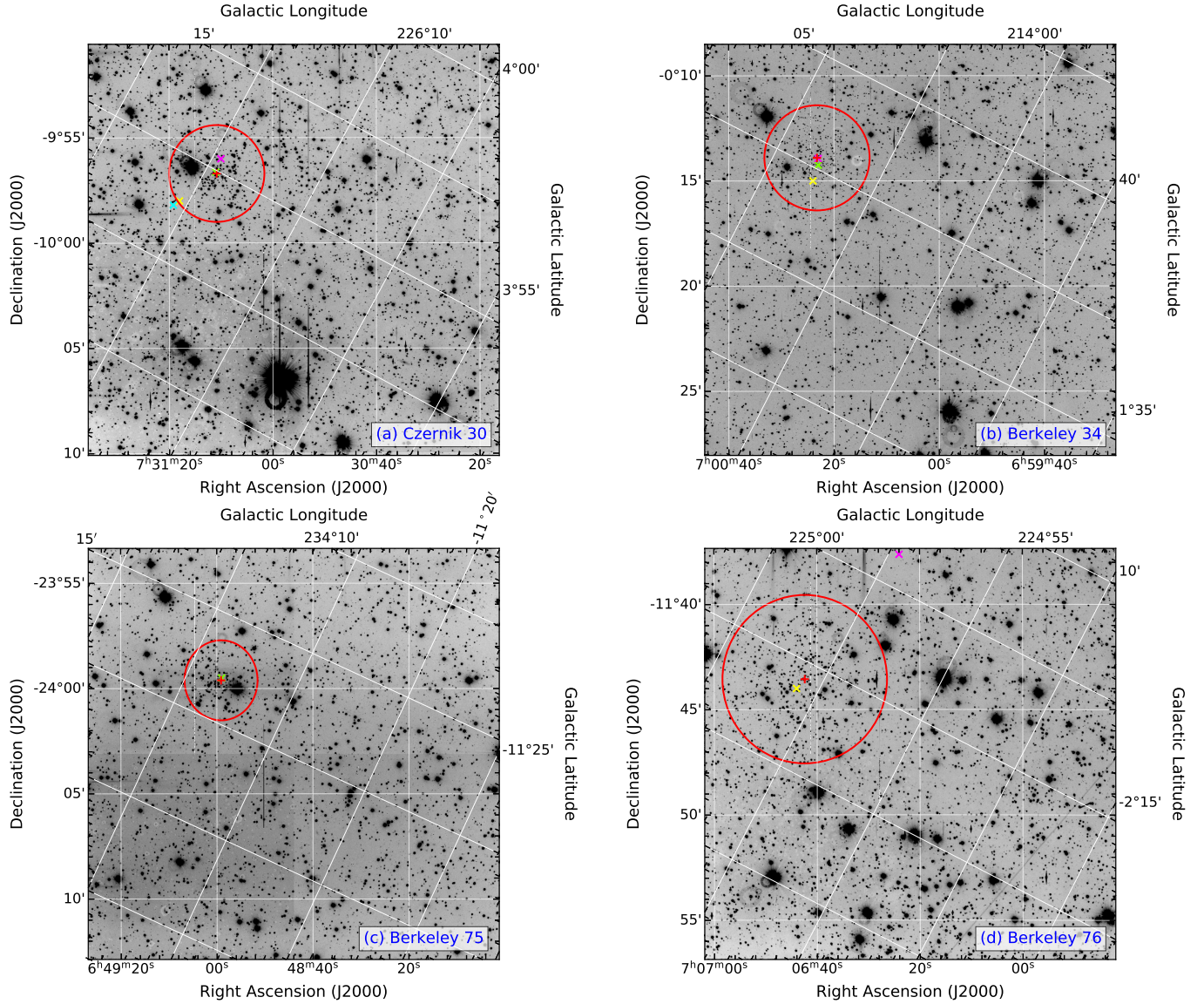


Figure 1. *B*-band images of the four old open clusters: (a) Czernik 30, (b) Berkeley 34, (c) Berkeley75, and (d) Berkeley 76. North is up, and east is to the left. The red cross symbols are the centers of the clusters, red circles show the scope of the clusters with the radii determined in this study. The radius for each cluster is shown in Tab. 2. Other X symbols indicate the centers of the clusters from previous studies (see the text for details).

3.3. Radius

We investigated the radial density profiles using concentric circles around the center of the cluster determined in the previous subsection, with a radial bin size of $0.5'$, as shown in Fig. 4. We counted the number of stars for each bin and divided it by the corresponding area (black line in Fig. 4). Since we located Czernik 30 in the upper right quadrant of the CCD chip during the observations, at around $> 6'$ the whole annulus was not covered in the image, so we could use only part of the annulus for the calculation.

For the member stars of Czernik 30, we plotted the radial density profile (blue line in Fig. 4) in the same way as we mentioned above. We decided $2.3' \pm 0.3'$ is the radius where the member fraction is greater than 0.5, since mem-

ber stars are the majority within the radius. The uncertainty was measured by the bootstrap method. Although a small number of member stars exist at $2.3' < r < 5'$, the number of field stars is much larger than the member stars in this region. In our study, we only used the stars within the radius to determine the physical parameters of Czernik 30.

This result, within the error range, is an excellent agreement with that of Hayes et al. (2015). While Piatti et al. (2009) used $r \sim 1.33'$ for the radius of Czernik 30 to get a clean sample of cluster stars, Hasegawa et al. (2008) did not mention any radius used in their study.

3.4. Reddening and Distance

We plot the *V* vs. *B* − *V* and *V* vs. *V* − *I* CMDs in Fig. 5, that shows the distinct main sequence (MS) and some

Table 1. Summary of the physical parameters

R.A. (J2000)	Dec. (J2000)	$E(B - V)$	$E(V - I)$	Age	[Fe/H]	$(m - M)_0$	Distance	Source
hh:mm:ss	dd:mm:ss	mag	mag	Gyr	dex	mag	kpc	
(a) Czernik 30								
07:31:10	−9 : 56	...	0.34	2.5	−0.4	14.27	...	Hasegawa et al. (2008)
07:31:18	−09 : 58 : 00	0.26 ± 0.02	...	$2.5^{+0.3}_{-0.25}$	-0.4 ± 0.2	...	6.2 ± 0.8	Piatti et al. (2009)
07:31:19.2	−09 : 58 : 12	0.5 ± 0.1	...	$0.8^{+0.5}_{-0.3}$	-0.3 ± 0.4	...	$7.9^{+1.6}_{-1.3}$	Perren et al. (2015)
07:31:11	−09 : 56 : 38	0.24 ± 0.06	0.36 ± 0.04	2.8 ± 0.3	-0.2 ± 0.15	...	6.5	Hayes et al. (2015)
07:31:10.8	−09 : 56 : 42	0.15 ± 0.08	0.27 ± 0.20	2.82 ± 0.32	-0.22 ± 0.15	14.05 ± 0.13	6.46 ± 0.39	This study
(b) Berkeley 34								
07:00:24	−00 : 15 : 00	0.45	0.60	2.8	−0.02	14.31	...	Hasegawa et al. (2004)
07:00:23	−00 : 14 : 15	0.30 ± 0.05	...	2.3 ± 0.4	−0.41	...	7.8 ± 0.8	Ortolani et al. (2005)
07:00:23	−00 : 13 : 56	$0.57 - 0.64$...	$2.1 - 2.5$	−0.31	$14.1 - 14.3$	$6 - 7$	Donati et al. (2012)
07:00:23.2	−00 : 13 : 54	0.56 ± 0.24	0.73 ± 0.31	2.51 ± 0.30	-0.30 ± 0.15	14.13 ± 0.19	6.70 ± 0.59	This study
(c) Berkeley 75								
06:48:59	−23 : 59 : 30	0.08 ± 0.05	0.13 ± 0.05	3.0 ± 0.3	−0.72	14.9	9.8	Carraro et al. (2005)
...	...	0.04 ± 0.03	...	4.0 ± 0.4	-0.22 ± 0.20	14.90 ± 0.20	9.1	Carraro et al. (2007)
06:48:59	−23 : 59 : 30	−0.38	Cantat-Gaudin et al. (2016)
06:48:59.1	−23 : 59 : 36	0.07 ± 0.18	0.13 ± 0.32	3.16 ± 0.73	-0.57 ± 0.20	14.44 ± 0.17	7.73 ± 0.61	This study
(d) Berkeley 76								
07:06:44	−11 : 44	...	0.70	1.6	−0.4	14.39	...	Hasegawa et al. (2008)
07:06:24	−11 : 37 : 38	0.73	...	0.8	2.505 ± 0.115	Tadross (2008)
07:06:24	−11 : 37 : 00	0.55 ± 0.10	0.75 ± 0.10	1.5	...	17.20 ± 0.15	12.6	Carraro et al. (2013)
07:06:42.4	−11 : 43 : 33	0.41 ± 0.33	0.57 ± 0.46	1.26 ± 0.14	0.00 ± 0.20	13.97 ± 0.23	6.22 ± 0.66	This study

Table 2. Galactic coordinates and radii of the four OCs

Name	Galactic longitude (l)	Galactic latitude (b)	Radius	Source
	[deg]	[deg]	[arcmin]	
Czernik 30	226.34	4.16	2.3 ± 0.3	This study
Berkeley 34	214.16	1.89	2.5 ± 0.3	This study
Berkeley 75	234.30	−11.19	1.9 ± 0.2	This study
Berkeley 76	225.10	−1.99	4.0 ± 0.3	This study

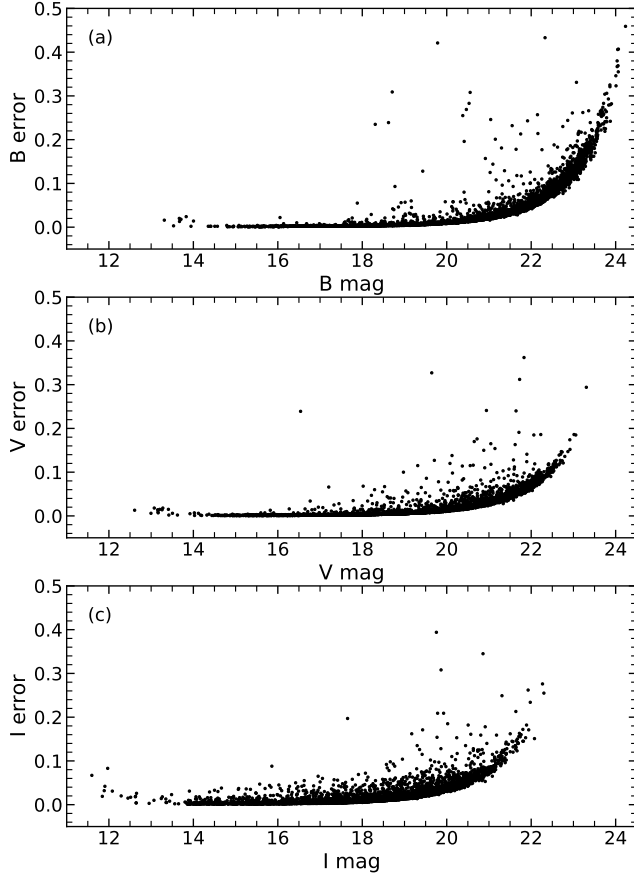
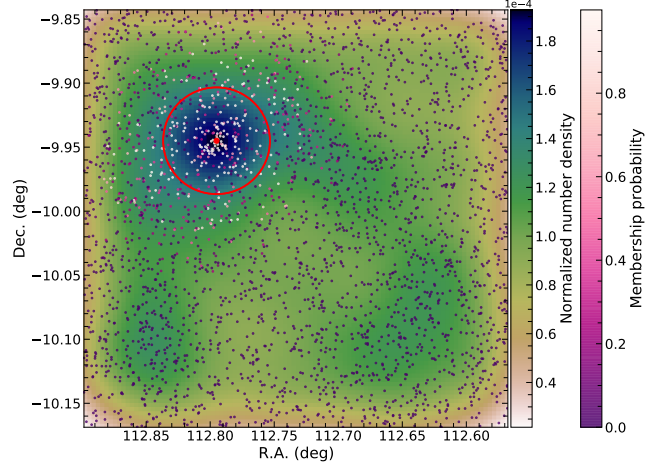
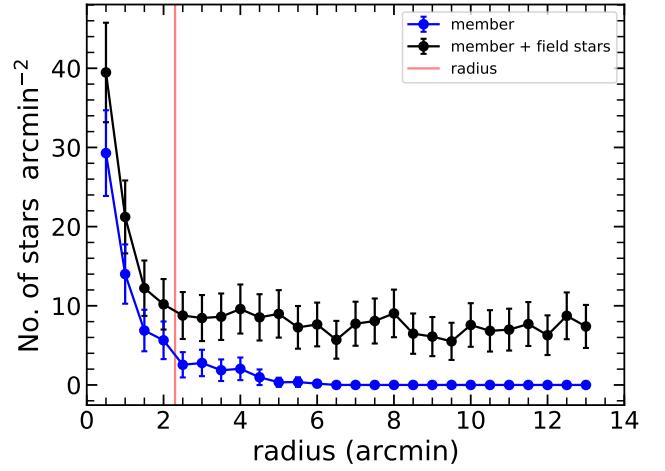
red clump (RC) stars. MS turn off (MSTO) is found to be located at $V \sim 18.05 \pm 0.05$ mag. We consider the three stars near $V \sim 15.51$ mag, $B - V \sim 1.16$ mag and $V - I \sim 1.30$ to be the RC stars. In the previous study, Piatti et al. (2009) inferred RC was located at $T_1 \sim 14.5 - 15.0$, $C - T_1 \sim 2.4 - 2.6$ in the Washington photometric System. The location of RC from Piatti et al. (2009) can be transformed into $V \sim 15.14 - 15.69$ and $V - I \sim 1.27 - 1.36$ using the

transformation equations of Bessell (2001), and these ranges include the location of the RC from our study.

RC stars are low-mass stars in the stage of core-helium burning, and they appear as a distinct grouping in the CMD (Cannon 1970; Girardi 2016). Since the magnitude and color of the RC stars are known to be constant, they have been widely used to get distances and reddenings for old OCs (Janes & Phelps 1994; Girardi 2016). The strength of using 2MASS (Two Micron All Sky Survey) (Skrutskie et al. 2006)

Table 3. Log of the observations for the four OCs

Target	Date	Filter	Exposure time
	(UT)		(seconds)
Czernik 30	2010 December 13	<i>B</i>	1200 s \times 3
		<i>V</i>	900 s \times 3
		<i>I</i>	800 s \times 3
Berkeley 34	2010 December 15	<i>B</i>	1200 s \times 3
		<i>V</i>	900 s \times 3
		<i>I</i>	900 s \times 3
Berkeley 75	2010 December 12	<i>B</i>	900 s \times 3
		<i>V</i>	900 s \times 2
		<i>I</i>	400 s \times 3
Berkeley 76	2010 December 12	<i>B</i>	1200 s \times 3
		<i>V</i>	900 s \times 3
		<i>I</i>	800 s \times 3

**Figure 2.** Error plot of the *BVI* bands for Czernik 30.**Figure 3.** Distribution function of the stellar photometry data from the *B*-band image including Czernik 30. The color bars on the right show the values of the normalized number density for the background (left) and the membership probability for the colors of dots (right). Black dots are the locations of stars without consideration of their brightnesses, red dot is the obtained center of Czernik 30 and the red circle is radius $2.3'$.**Figure 4.** Radial density profile of Czernik 30. While the blue line includes only the member stars, the black line includes members and field stars. The red vertical line is the adopted radius of Czernik 30. The error bars indicate the Poisson errors.

K_s -band of the RC stars comes from the smaller dependency on age, metallicity, and extinction than other optical bands. The absolute magnitude and intrinsic color of the RC stars have been studied by many researchers (Alves 2000; Grocholski & Sarajedini 2002; van Helshoecht & Groenewegen 2007; Groenewegen 2008; Laney et al. 2012; Francis & Anderson 2014; Girardi 2016; Chen et al. 2017; Hawkins et al. 2017; Ruiz-Dern et al. 2018; Chan & Bovy 2020). We use the absolute magnitude of $M_{K_s} = -1.628 \pm 0.133$ and the intrinsic color $(J - K_s)_{RC,0} = 0.656 \pm 0.040$ for the RC stars from the

most recent study of Wang & Chen (2021). They used the *Gaia* EDR3 data, the Apache Point Observatory Galactic Evolution Experiment (APOGEE) and the Large Sky Area Multi-Object Fiber Spectroscopic Telescope (LAMOST) data and 156,000 RC samples to calculate the absolute magnitude and intrinsic color of the RC stars. We matched our RC stars with the 2MASS JHK_s band catalog data. The list of the three RC stars of Czernik 30 is shown in Tab. 4. The mean magnitude and color of the RC stars of Czernik 30 are $V = 15.54 \pm 0.10$, $B - V = 1.15 \pm 0.07$, $J = 13.19 \pm 0.01$, $H = 12.60 \pm 0.02$, $K_s = 12.46 \pm 0.01$, and $J - K_s = 0.73 \pm 0.01$.

Using the intrinsic $(J - K_s)$ color of the RC stars derived by Wang & Chen (2021), we obtain the reddening value of $E(J - K_s) = (J - K_s)_{RC} - (J - K_s)_{RC,0} = 0.07 \pm 0.04$ and $E(B - V) = 0.15 \pm 0.08$ using the relation $E(J - K_s) = 0.488 \times E(B - V)$ (Kim 2006). We also use the δV index to obtain the reddening value, which is defined as the difference between the magnitudes of RC and MSTO (Phelps et al. 1994; Janes & Phelps 1994; Kim & Sung 2003). When $\delta V > 1.0$, the RC of an OC has and the absolute magnitude of $M_{V,RC} = 0.90 \pm 0.40$ and the intrinsic color of $(B - V)_0 = 0.95 \pm 0.10$ (Janes & Phelps 1994). Since, δV is 2.54 mag for Czernik 30, the reddening value is derived to be $E(B - V) = (B - V) - (B - V)_0 = 0.20 \pm 0.12$ which agrees with the reddening value from the RC method within the error range.

Using the mean K_s magnitude of 12.46 ± 0.01 for the RC stars of Czernik 30, the distance modulus is derived to be $(m - M)_0 = K_s - M_{K_s} - A_{K_s} = 14.05 \pm 0.13$ mag ($d = 6.46 \pm 0.39$ kpc), where $A_{K_s} = 0.528 \times E(J - K_s)$ (Nishiyama et al. 2009).

3.5. Age and $[Fe/H]$

To derive the physical parameters of age and metallicity for Czernik 30, we have performed PARSEC isochrone fittings (Bressan et al. 2012) with the distance and reddening values fixed, which were obtained in Sec. 3.4. From the best fitted PARSEC isochrone shown in Fig. 5 (a), we obtained age and metallicity and their uncertainties from the possible isochrone variations within a tolerable limit: $\log t = 9.45 \pm 0.05$ ($t = 2.82 \pm 0.32$ Gyr), $[Fe/H] = -0.22 \pm 0.15$ dex. We derived $\log t = 9.45 \pm 0.05$ ($t = 2.82 \pm 0.32$

Gyr), $E(V - I) = 0.27 \pm 0.20$ from the best fitted PARSEC isochrone in V vs. $(V - I)$ CMD (Fig. 5 (b)).

3.6. Comparison with previous studies

There are four previous studies about the physical parameters of Czernik 30. The physical parameters from the previous studies and our study are shown in Table 1.

Hasegawa et al. (2008) used the Padova isochrones and estimated age $t = 2.5$ Gyr ($\log t = 9.40$), metallicity $Z = 0.008$ ($[Fe/H] = -0.41$), color excess $E(V - I) = 0.34$, and distance modulus $(m - M)_0 = 14.27$. Piatti et al. (2009) used three radii to determine the physical parameters: r_{FWHM} , r_{clean} and r_{cls} (see details in sec. 3 of Piatti et al. (2009)), and obtained age $t = 2.5^{+0.30}_{-0.25}$ Gyr ($\log t = 9.40$), metallicity $[Fe/H] = -0.4 \pm 0.2$, color excess $E(B - V) = 0.26 \pm 0.02$ and distance $d = 6.2 \pm 0.8$ kpc using the Padova isochrones. Perren et al. (2015) developed a code that automatically estimates the physical parameters of OCs after finding the center, and they obtained the physical parameters of 20 OCs including Czernik 30 using their code. Perren et al. (2015) presented two types of radii: one was a manually determined radius and the other was automatically assigned by the code. They suggested two physical parameter sets using the two radii, and these two physical parameter sets are overall not in good agreement, among which only the distance values are quite similar. Adopting their values obtained with the automatically found radius, $E(B - V)$ and age from their study were 0.35 mag larger and 2.02 Gyr younger, respectively, than those in our study, and they suggested ~ 1.4 kpc farther distance than that in our study. Hayes et al. (2015) analyzed the photometric and spectroscopic data of Czernik 30 and determined age $t = 2.8 \pm 0.3$ Gyr ($\log t = 9.45$), metallicity $[Fe/H] = -0.2 \pm 0.15$, distance modulus $(m - M)_V = 14.8 \pm 0.1$ ($d \sim 6.5$ kpc), and color excess $E(B - V) = 0.24 \pm 0.06$ and $E(V - I) = 0.36 \pm 0.04$.

In this study, we have used both the RC properties and the isochrone fitting. While our study obtained somewhat smaller reddening values compared to the previous studies, age, metallicity, and distances are in very good agreement with the values in the literature.

Table 4. The photometry results of the red clump stars for the four old OCs

ID	R.A.	Dec.	B	B error	V	V error	I	I error	J	J error	H	H error	K _s	K _s error
	hh:mm:ss	dd:mm:ss	mag	mag	mag	mag	mag	mag	mag	mag	mag	mag	mag	mag
(a) Czernik 30														
3779	07:31:07.28	-09 : 55 : 03.2	16.629	0.002	15.480	0.001	14.183	0.003	13.198	0.027	12.610	0.022	12.457	0.026
3800	07:31:07.47	-09 : 55 : 51.0	16.637	0.002	15.481	0.002	14.191	0.005	13.180	0.070	12.579	0.090	12.456	0.069
4128	07:31:10.98	-09 : 56 : 48.3	16.727	0.002	15.560	0.001	14.260	0.005	13.191	0.027	12.615	0.022	12.468	0.026
(b) Berkeley 34														
3657	07:00:16.37	-00 : 12 : 29.4	18.309	0.005	16.743	0.002	15.032	0.002	13.620	0.028	12.875	0.031	12.692	0.024
3870	07:00:19.12	-00 : 12 : 39.5	18.338	0.006	16.760	0.002	15.055	0.003	13.636	0.035	12.982	0.039	12.726	0.029
4137	07:00:21.97	-00 : 14 : 38.9	18.306	0.004	16.726	0.002	14.971	0.003	13.599	0.032	12.880	0.034	12.673	0.026
4273	07:00:23.22	-00 : 15 : 40.5	18.267	0.004	16.660	0.002	14.896	0.002	13.461	0.033	12.717	0.032	12.502	0.028
(c) Berkeley 75														
2525	06:49:00.11	-23 : 59 : 39.7	16.582	0.002	15.547	0.002	14.433	0.002	13.577	0.035	13.039	0.044	12.893	0.041
2710	06:49:02.99	-23 : 59 : 29.6	16.300	0.002	15.328	0.002	14.237	0.002	13.473	0.037	12.917	0.041	12.772	0.043
(d) Berkeley 76														
3582	07:06:36.28	-11 : 44 : 23.6	17.723	0.003	16.320	0.002	14.717	0.002	13.410	0.029	12.710	0.023	12.527	0.026
4109	07:06:42.60	-11 : 43 : 32.5	17.624	0.003	16.255	0.002	14.710	0.002	13.354	0.024	12.744	0.027	12.527	0.029
4149	07:06:43.02	-11 : 43 : 05.8	17.523	0.002	16.155	0.002	14.573	0.002	13.319	0.030	12.674	0.031	12.471	0.030
4331	07:06:45.14	-11 : 43 : 55.6	17.206	0.002	15.878	0.004	14.291	0.002	13.001	0.028	12.341	0.029	12.086	0.021
4352	07:06:45.42	-11 : 46 : 49.3	17.658	0.003	16.275	0.002	14.660	0.002	13.338	0.029	12.691	0.031	12.499	0.027

NOTE—*J, H, K_s* magnitudes and magnitude errors are from the 2MASS catalog (Skrutskie et al. 2006).

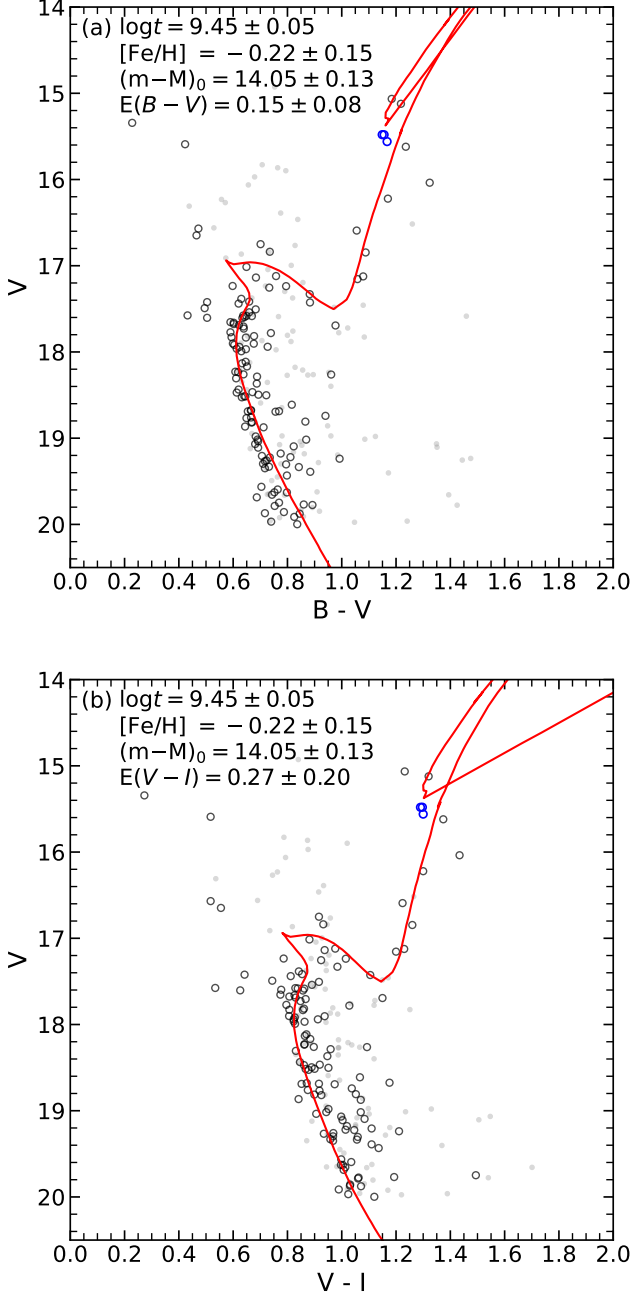


Figure 5. Best fit PARSEC isochrone line on (a) V vs. $(B - V)$ CMD and (b) V vs. $(V - I)$ CMD of Czerwik 30. The black open circle symbols are the member stars of Czerwik 30, the blue open circles indicate the RC stars of Czerwik 30, the gray dots are non-member stars but located inside the radius of Czerwik 30 and the red lines are the best fit PARSEC isochrone model.

4. BERKELEY 34

In the same way as in Czerwik 30, we determined the center of Berkeley 34: $\alpha_{J2000} = 07^h00^m23.2^s$ and $\delta_{J2000} = -00^\circ13'54''$ (red cross symbol in Fig. 1 (b)) using *gaussian_kde* package and the distribution function shown in

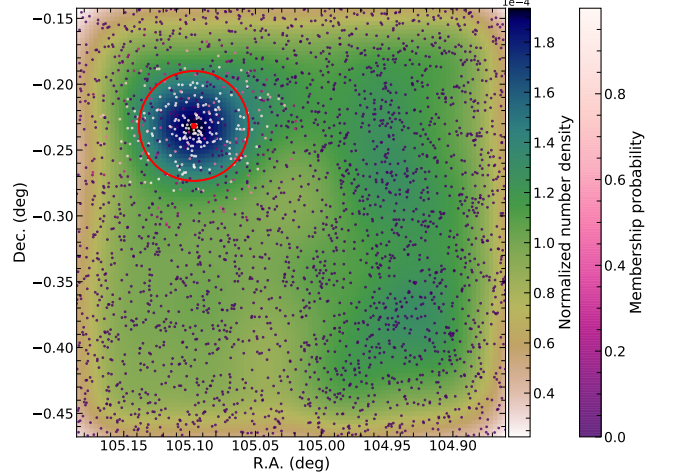


Figure 6. Distribution function of the stellar photometry data from the B -band image including Berkeley 34. Black dots are the locations of stars without consideration of their brightnesses, and the red dot indicates the center of Berkeley 34 obtained from Gaussian fitting. The red circle indicates the radius $2.5'$ of Berkeley 34. The white-magenta dot symbols are the members of Berkeley 34. The left color bar shows values of the normalized number density function and the right color bar the membership probability for each star.

Fig. 6. The center of Berkeley 34 from the previous study is shown in Fig. 1 (b). The green x symbol is $\alpha_{J2000} = 07^h00^m23^s$, $\delta_{J2000} = -00^\circ14'15''$ (Ortolani et al. 2005) and the yellow x symbol is $\alpha_{J2000} = 07^h00^m24^s$, $\delta_{J2000} = -00^\circ15'00''$ (Hasegawa et al. 2004). Donati et al. (2012) presents $\alpha_{J2000} = 07^h00^m23^s$, $\delta_{J2000} = -00^\circ13'56''$ as the center of Berkeley 34, and the magenta x symbol indicates this location.

To select the member stars of Berkeley 34, we adopted the pyUPMASK package (see Section 3.2) using the *Gaia* proper motion and parallax data. Finally, 147 stars were selected as the members of Berkeley 34 and are shown in Fig. 6 as white-magenta dot symbols.

Fig. 7 shows the radial density profile of Berkeley 34. We determine the radius of Berkeley 34 to be about $2.5' \pm 0.3'$ where the member fraction is greater than 0.5 in spite of the existence of members from $2.5'$ to $4'$. While Hasegawa et al. (2004) did not specify the radius value adopted in their study, Ortolani et al. (2005) used $r \sim 58''$ in fitting the isochrones, and Donati et al. (2012) used the stars inside $r \sim 2.5'$ region.

Fig. 8 shows V vs. $B - V$ and V vs. $V - I$ CMDs for the stars in $r \sim 2.5'$. The MSTO is located at $V \sim 19.00$ mag, $B - V \sim 0.98$, and $V - I \sim 1.25$. Hasegawa et al. (2004) estimated the MSTO location to be $(V, V - I) = (18.5, 1.2)$. Donati et al. (2012) claimed two points for the MS of Berkeley 34: MS red hook (the reddest part of MS) at $V \sim 18.5$ mag and the MS termination point at $V \sim 18.0$ mag.

We took the four stars near $V \sim 16.72$, $B - V \sim 1.58$, and $V - I \sim 1.73$ as the RC stars of Berkeley 34, and their photometry data are shown in Table 4. From the RC method, we calculate the reddening values $E(J - K_s) =$

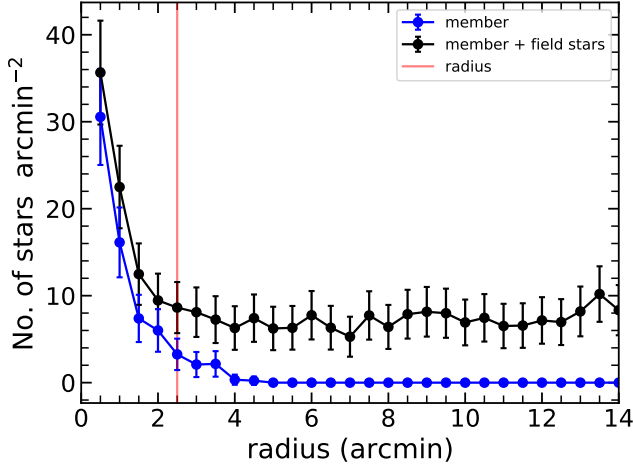


Figure 7. Radial density profile of Berkeley 34. The black line indicate the radial density profile of member stars and field stars. The blue line indicate the radial density profile of member stars. The red vertical line is the radius of Berkeley 34. The error bars indicate the Poisson errors.

0.27 ± 0.12 , $E(B - V) = 0.56 \pm 0.24$, and the distance modulus $(m - M)_0 = 14.13 \pm 0.19$ ($d = 6.70 \pm 0.59$ kpc). Since δV index is 2.28, $E(B - V)$ was estimated to be 0.63 ± 0.10 , which is consistent with the value from the RC method. Donati et al. (2012) suggested two groups of RC, brighter and fainter: the position of the brighter RC group was at $V \sim 15.7$ and $B - V \sim 1.7$ and the fainter RC group was located at $V \sim 16.7$ and $B - V \sim 1.55$. We consider only one RC group exists for Berkeley 34, which corresponds to the fainter group in Donati et al. (2012).

We tried to fit the PARSEC isochrones to the CMDs of Berkeley 34 using the reddening and distance modulus derived using the RC method. Fig. 8 shows the best fit PARSEC isochrones with CMDs. Finally, we determined the fundamental physical parameters for Berkeley 34, which include age, metallicity, distance modulus, and color excess: age $\log t = 9.40 \pm 0.05$ ($t = 2.51 \pm 0.30$ Gyr), metallicity $[\text{Fe}/\text{H}] = -0.30 \pm 0.15$ dex, distance modulus $(m - M)_0 = 14.13 \pm 0.19$ ($d = 6.70 \pm 0.59$ kpc), and color excesses $E(B - V) = 0.56 \pm 0.24$ and $E(V - I) = 0.73 \pm 0.31$.

As shown in Table 1, Hasegawa et al. (2004) obtained age $t = 2.8$ Gyr, metallicity $Z = 0.019$ ($[\text{Fe}/\text{H}] = -0.02$), distance $(m - M)_0 = 14.31$, and color excesses $E(B - V) = 0.45$ and $E(V - I) = 0.60$. Ortolani et al. (2005) obtained the distance to Berkeley 34 of $d = 7.8 \pm 0.8$ kpc. Donati et al. (2012) measured the physical parameters using Full Spectrum of Turbulence (FST), Padova, Frascati Raphson Newton Evolutionary Code (FRANEC) isochrone. They gave a physical parameters range from the FST isochrone: age from 2.1 to 2.5 Gyr, metallicity $Z = 0.01$ ($[\text{Fe}/\text{H}] = -0.31$ dex), distance from 6 to 7 kpc ($(m - M)_0 \sim 14.1 - 14.3$), color excess $E(B - V) \sim 0.57 - 0.64$. Overall, our results show good agreement with the values in the three studies listed above.

5. BERKELEY 75

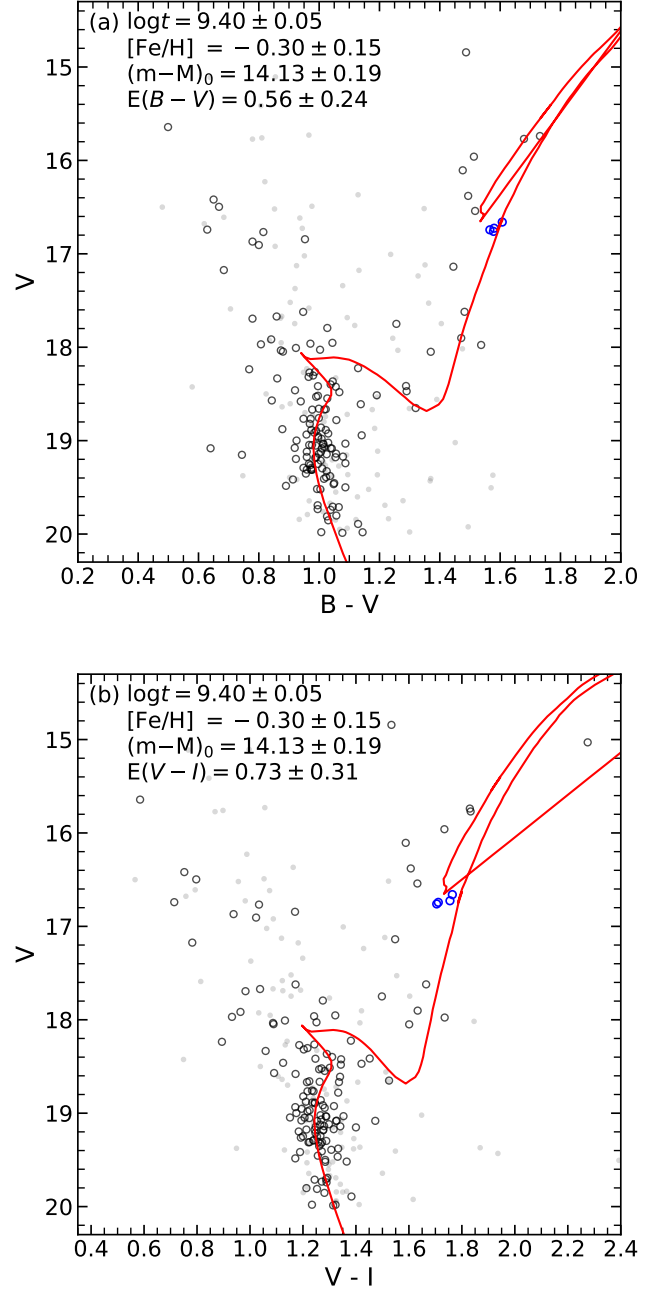


Figure 8. Best fit PARSEC isochrone on V vs. $(B - V)$ CMD (panel (a)) and V vs. $(V - I)$ CMD (panel (b)) of Berkeley 34. The black open circles are the member stars of Berkeley 34, the blue open circles are the RC of Berkeley 34, the gray dot symbols are non-member stars but located inside the radius of Berkeley 34 and the red line is the best fitted PARSEC isochrone model.

In the same way as in Czernik 30, we determined the center of Berkeley 75 using the kernel density estimation method (Fig. 9). Berkeley 75 is located at $\alpha_{J2000} = 06^h 48^m 59.1^s$, $\delta_{J2000} = -23^\circ 59' 36''$. The green x symbol in Fig. 1 (c) for

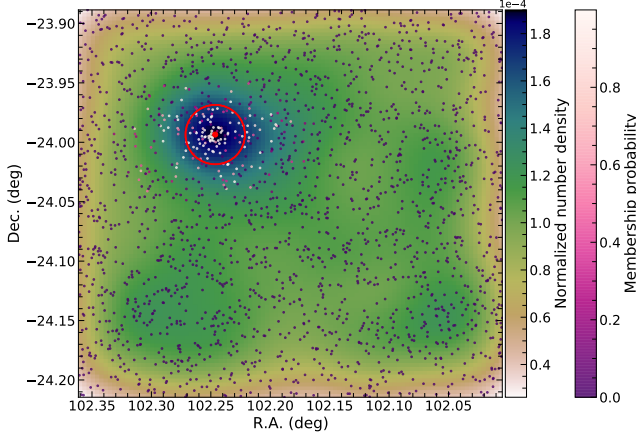


Figure 9. Distribution function of the stellar photometry data from the B -band image including Berkeley 75. The black dots are the locations of stars without considering their brightnesses, the red dot is the center of Berkeley 75 and the red circle indicates the radius $1.9'$ of Berkeley 75. The white-magenta dot symbols are the members of Berkeley 75. The left color bar shows the values of the normalized number density function and the right color bar the membership probability for each star.

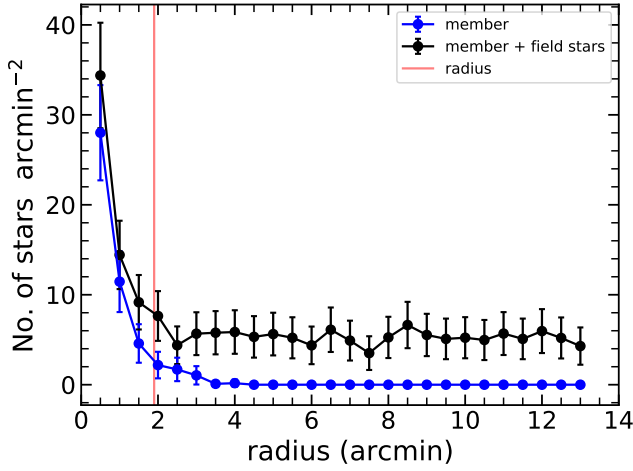


Figure 10. Radial density profile of Berkeley 75. The black line includes the member stars and the field stars, and the blue line is the radial density profile of members. The red line indicates the radius of Berkeley 75. The error bars indicate the Poisson errors.

$\alpha_{J2000} = 06^h48^m59^s$ and $\delta_{J2000} = -23^\circ59'30''$ indicates the center position of Berkeley 75 used by Carraro et al. (2005).

By adopting the pyUPMASK package (see Section 3.2), 77 stars were determined to be the members of Berkeley 75. The radial density profile of Berkeley 75 is shown in Fig. 10. The region from $1.9'$ to $4'$ has member stars of Berkeley 75 but field stars represent the majority in this region. Thus, we determined the radius of Berkeley 75 to be $1.9'$. Carraro et al. (2005) determined the radius of Berkeley 75 to be $1'$ from its radial density profile.

The CMDs of Berkeley 75 are shown in Fig. 11, where MSTO is located at $V \sim 18.1$ mag, $B - V \sim 0.46$, and $V - I \sim 0.63$. Carraro et al. (2005) also presented almost the same value ($V \approx 18$ mag) for the MSTO.

We selected two RC stars of Berkeley 75, which are listed in Table 4 (c). The mean magnitude and color for the RC stars in Berkeley 75 are $V = 15.44 \pm 0.11$, $B - V = 1.00 \pm 0.18$, and $V - I = 1.10 \pm 0.15$ while Carraro et al. (2005) measured the location of the RCs to be $V \sim 16.0$ mag which is quite different from ours. Using the RC method, we calculated the distance $(m - M)_0 = 14.44 \pm 0.17$ ($d = 7.73 \pm 0.61$ kpc) and reddening $E(B - V) = 0.07 \pm 0.18$. Using δV index of 2.66 and the method of Janes & Phelps (1994), we obtained $E(B - V) = 0.05 \pm 0.20$, which is consistent with the value from the RC method within error range.

We tried to determine the age and metallicity of Berkeley 75 using the PARSEC isochrones and the reddening and distance values obtained from the RC method, as shown in Fig. 11. We measured age $\log t = 9.50 \pm 0.10$ ($t = 3.16 \pm 0.73$ Gyr), metallicity $[\text{Fe}/\text{H}] = -0.57 \pm 0.20$ dex, distance modulus $(m - M)_0 = 14.44 \pm 0.17$, and color excesses $E(B - V) = 0.07 \pm 0.18$ and $E(V - I) = 0.13 \pm 0.32$. Although the reddening value measured by Janes & Phelps (1994) was not exactly consistent with the reddening value from the RC method, the reddening values were consistent with the values from the RC method within the error range. Carraro et al. (2005) obtained distance modulus $(m - M) = 15.2$, color excesses $E(B - V) = 0.08$ and $E(V - I) = 0.13$ using the Padova isochrones of age 3 Gyr and metallicity $Z = 0.004$ ($[\text{Fe}/\text{H}] = -0.72$ dex). Carraro et al. (2007) revised the estimates to be: age 4.0 ± 0.4 Gyr, metallicity $[\text{Fe}/\text{H}] = -0.22 \pm 0.20$ dex, distance modulus $(m - M) = 14.90 \pm 0.20$, and color excess $E(B - V) = 0.04 \pm 0.03$. The revised parameters of Carraro et al. (2007) show good agreement with our parameters.

6. BERKELEY 76

Using the kernel density estimation method as in the previous sections, we determined the center of Berkeley 76 as shown in Fig. 12. Unlike the three OCs in the previous sections, Berkeley 76 has many more number of stars spread in the field. We determined the center of Berkeley 76 to be at $\alpha_{J2000} = 07^h06^m42.4^s$ and $\delta_{J2000} = -11^\circ43'33''$. Carraro et al. (2013) suggested the center of Berkeley 76 to be $\alpha_{J2000} = 07^h06^m24^s$ and $\delta_{J2000} = -11^\circ37'00''$. However, since their Fig. 1 and our Fig. 1 (d) show the same region, their center coordinates in their Table 1 might not be correct. The yellow x symbol in our Fig. 1 (d) indicates $\alpha_{J2000} = 07^h06^m44^s$ and $\delta_{J2000} = -11^\circ44'$ from Hasegawa et al. (2008) and the magenta x symbol is $\alpha_{J2000} = 07^h06^m24^s$ and $\delta_{J2000} = -11^\circ37'38''$ from Tadross (2008). The center location from Tadross (2008) is quite far away ($7.51'$) from the center in our study.

288 stars are selected as members of Berkeley 76 from the pyUPMASK algorithm (Pera et al. 2021) with *Gaia* EDR3 proper motion and parallax data. In Fig. 13, the trend in the radial density profile of Berkeley 76 is different from those in the three OCs of the previous sections. $4.0' \pm 0.3'$ is determined to be the radius of Berkeley 76 where the member fraction is 0.5. Carraro et al. (2013) used $2'$ as the radius of

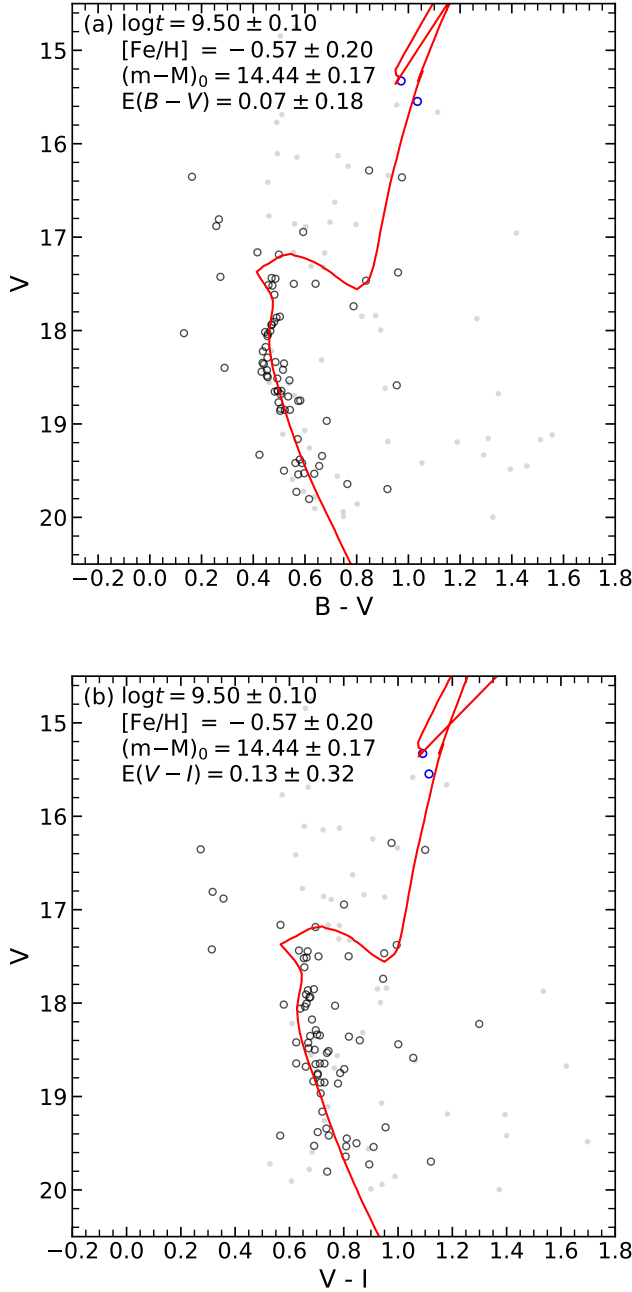


Figure 11. Best fit PARSEC isochrone on V vs. $(B - V)$ CMD (panel (a)) and V vs. $(V - I)$ CMD (panel (b)) of Berkeley 75. The black open symbols are the member stars of Berkeley 75, the blue open symbols are the RC stars of Berkeley 75, the gray dots are non-member stars but located inside the radius of Berkeley 75 and the red lines are the best fit PARSEC isochrone model for each CMD.

Berkeley 76 and [Tadross \(2008\)](#) obtained $4.5'$ for the radius of Berkeley 76.

Fig. 14 shows the V vs. $B - V$ and V vs. $V - I$ CMDs for Berkeley 76, where the five RC stars can be seen at $V \sim 16.22 \pm 0.08$, $B - V \sim 1.35 \pm 0.06$, and $V - I \sim 1.59 \pm 0.03$. The photometry results for these five stars are shown in Tab. 4

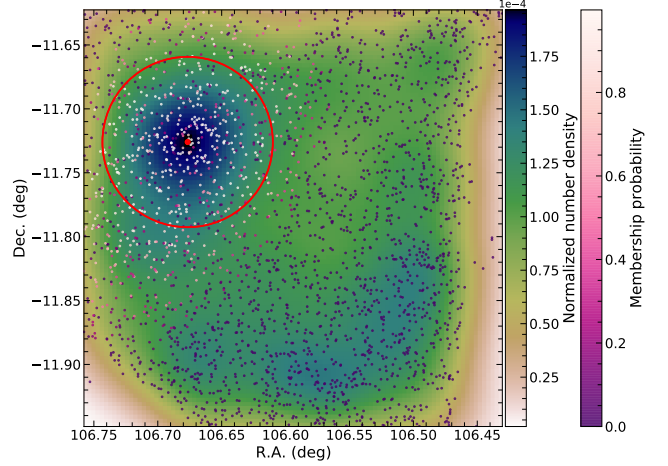


Figure 12. Distribution function of the stellar photometry data from the B -band image including Berkeley 76. The black dots are the locations of stars without considering their brightnesses, the red dot is the center of Berkeley 76 and the red circle is the radius $4.0'$ of Berkeley 76. The white-magenta dot symbols are the members of Berkeley 76. The left color bar shows values of the normalized number density function and the right color bar the membership probability for each star.

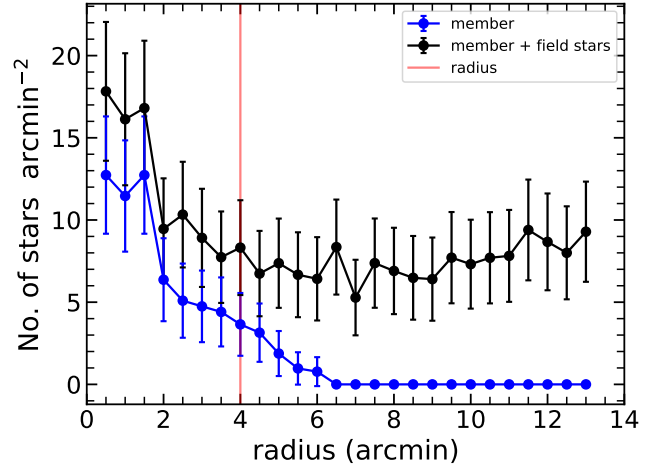


Figure 13. Radial density profile of Berkeley 76. The black line includes the member stars and the field stars, and the blue line is the radial density profile of members. The red line indicates the radius of Berkeley 76. The error bars indicate the Poisson errors.

(d). We determined the distance and reddening of Berkeley 76 using the RC method: distance modulus $(m - M)_0 = 13.97 \pm 0.23$ and reddening $E(B - V) = 0.41 \pm 0.33$. δV index of Berkeley 76 is 2.04, and this gives us $E(B - V) = 0.39 \pm 0.12$ which is consistent with that from the RC method.

[Carraro et al. \(2013\)](#) suggested the mean magnitude and color for the four RC stars in Berkeley 76 to be $V \sim 17.9$ and $B - V \sim 1.4$, respectively. While the $B - V$ colors are in very good agreement with their color and ours, their V

magnitude is ~ 1.7 mag fainter than ours. Considering two things, that (1) the two CMDs in our study (Fig. 14) and Carraro et al. (2013) (their Fig. 7) are very similar, and (2) the distance modulus estimated by Carraro et al. (2013) $((m - M)_0 = 17.20 \pm 0.15)$ is much larger than those of Hasegawa et al. (2008) $((m - M)_0 = 14.39)$ and our study $((m - M)_0 = 13.97 \pm 0.23)$, we suspect the V magnitudes in Carraro et al. (2013) were somehow shifted by $\sim +1.7$ mag.

We tried to find best fit PARSEC isochrones using the distance and the reddening values from the RC method as shown in Fig. 14. We determined the physical parameters: age $\log t = 9.10 \pm 0.05$ ($t = 1.26 \pm 0.14$ Gyr), metallicity $[\text{Fe}/\text{H}] = 0.00 \pm 0.20$ dex, distance modulus $(m - M)_0 = 13.97 \pm 0.23$ ($d = 6.22 \pm 0.66$ kpc), and color excesses $E(B - V) = 0.41 \pm 0.33$ and $E(V - I) = 0.57 \pm 0.46$.

7. RADIAL METALLICITY DISTRIBUTION

OCs can help reveal the chemical evolution of the Galactic disk (Netopil et al. 2016; Kim et al. 2017; Chen & Zhao 2020; Donor et al. 2020; Spina et al. 2021; Zhang et al. 2021; Netopil et al. 2022). Netopil et al. (2016) mentioned the importance of a homogeneous data set and they obtained the Galactic metallicity distribution from a homogeneous data set of 172 OCs for three ranges, which is divided at $R_{GC} \sim 9$ and 12 kpc. Donor et al. (2020) studied the chemical abundance distribution of the Galactic disk using OC data from the Sloan Digital Sky Survey/APOGEE DR 16, and they determined the $[\text{Fe}/\text{H}]$ vs R_{GC} has a slope of -0.068 ± 0.001 dex kpc^{-1} in the region of $6 < R_{GC} < 13.9$ kpc from the Markov Chain Monte Carlo method. Spina et al. (2021) found the slope of $[\text{Fe}/\text{H}]$ over R_{GC} to be -0.076 ± 0.009 dex kpc^{-1} using a bayesian regression with the spectroscopic data of 134 OCs from GALactic Archaeology with HERMES (GALAH) survey or APOGEE survey. Spina et al. (2022) gathered high-resolution spectroscopic surveys data and measured -0.064 ± 0.007 dex kpc^{-1} as the metallicity gradient. They also suggested a flat metallicity distribution at outside of $R_{GC} = 12.1 \pm 1.1$ kpc.

We combined the distances and the $[\text{Fe}/\text{H}]$ values from the following five catalogs, together with the data for the four OCs obtained in this study : Dias et al. (2002), Netopil et al. (2016), Donor et al. (2020), Spina et al. (2021), and Dias et al. (2021). Dias et al. (2002, 2021) are the OC catalogs including the physical parameters such as age, distance and metallicity. Netopil et al. (2016), Donor et al. (2020), and Spina et al. (2021) focused on the chemical evolution in the Galactic disk. If there were more than two $[\text{Fe}/\text{H}]$ values, we tried to use the values from the spectroscopic data, if they exist, expecting them to have higher accuracy. We used 8 kpc as the solar distance from the Galactic center, $R_{GC,\odot}$. The number of old OCs in the final catalog is 236.

Fig. 15 shows the Galactic radial metallicity distribution of the OCs with ages older or younger than 1 Gyr. We tried applying a single linear fit (panel (a)) and a broken linear fit (panel (b)) to the combined data for OCs with $t \geq 1$ Gyr. The broken linear fit assumes the existence of discontinuity and uses two linear functions for the fit, with the final result listed in Table 5. While the existence of the discontinuity is a controversial issue, several possibilities are suggested as

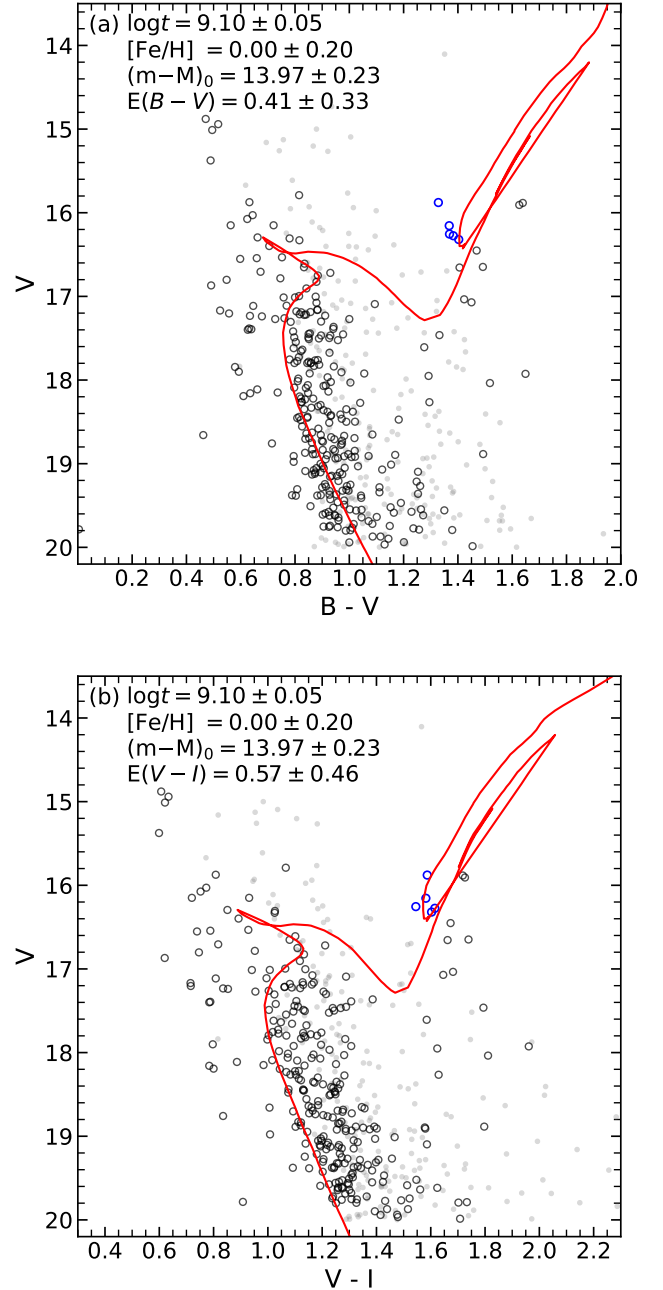


Figure 14. (a) V vs. $(B - V)$ and (b) V vs. $(V - I)$ CMDs of Berkeley 66 with the best fit PARSEC isochrones. The black symbols are the member stars of Berkeley 66, the blue open circles are the RC stars of Berkeley 66, the gray dots are non-member stars but located inside the radius of Berkeley 66 and the red solid lines are the best fitted PARSEC isochrone model.

causes of the metallicity distribution in the Galactic disk: for example, radial migration (Minchev et al. 2013, 2018; Zhang et al. 2021; Netopil et al. 2022), metal enrichment (Monteiro et al. 2021), etc.

The number of OCs younger than 1 Gyr shown in Fig. 15 (c) is negligible in the outer part of the Galactic disk, espe-

Table 5. The metallicity gradient from least square fit using 236 old OCs in Fig. 15

Function	Range	N	Gradient	Intercept
	kpc		dex kpc ⁻¹	dex
single linear fit		236	-0.052 ± 0.004	$+0.391 \pm 0.040$
broken linear fit	< 12	196	-0.070 ± 0.006	$+0.556 \pm 0.056$
broken linear fit	≥ 12	40	-0.016 ± 0.010	-0.101 ± 0.145

cially outside of 14.5 kpc. The small number of samples at the outer part in Fig. 15 (b) make the broken linear fit look more suitable than the single linear fit. For the broken linear fit in Fig. 15 (b), we tried to find the appropriate location of the discontinuity from 12 kpc to 14 kpc using a step size of 0.5 kpc. The discontinuity at 12 kpc has, naturally, the largest number of old OCs at the outer region, hence, the Bayesian information criteria (BIC)² value at 12 kpc was the smallest among those from 12 kpc to 14 kpc. When using the old OCs as elements to investigate the metallicity distribution in the Galactic disk, it is important to increase the number of samples at the outer region, especially outside of 14 kpc, for better analysis. Although the addition of the four old OCs from our study to Fig. 15 is not a significant increase in the number of the sample, our data are relatively important in that all the four clusters are located at the outer region of $r \sim 14$ kpc.

8. SUMMARY

In this paper, we investigated four old OCs in the MWG. We photometrically determined their physical quantities and compared them with those in previous studies. By combining data of the four OCs with those from previously known OCs, we newly estimated the radial metallicity distribution of the MWG. We summarize our results as follows (see also Table 1 and Table 2).

- We determined the center of Czernik 30 - $\alpha_{J2000} = 07^h31^m10.8^s$, $\delta_{J2000} = -09^\circ56'42''$. We estimated the physical parameters: radius $2.3' \pm 0.3'$, color excess $E(B - V) = 0.15 \pm 0.08$, age $t = 2.82 \pm 0.32$ Gyr ($\log t = 9.45 \pm 0.05$), metallicity $[\text{Fe}/\text{H}] = -0.22 \pm 0.15$ dex, and distance modulus $(m - M)_0 = 14.05 \pm 0.13$.
- We determined the center of Berkeley 34 - $\alpha_{J2000} = 07^h00^m23.2^s$, $\delta_{J2000} = -00^\circ13'54''$. We estimated the quantities: radius $2.5' \pm 0.3'$, color excess $E(B - V) = 0.56 \pm 0.24$, age $t = 2.51 \pm 0.30$ Gyr ($\log t = 9.40 \pm 0.05$), metallicity $[\text{Fe}/\text{H}] = -0.30 \pm 0.15$ dex, and distance modulus $(m - M)_0 = 14.13 \pm 0.19$.
- We determined the center of Berkeley 75 - $\alpha_{J2000} = 06^h48^m59.1^s$, $\delta_{J2000} = -23^\circ59'36''$. As for the physical quantities: radius $1.9' \pm 0.2'$, color excess $E(B - V) = 0.07 \pm 0.18$, age $t = 3.16 \pm 0.73$ Gyr ($\log t =$

9.50 ± 0.10), metallicity $[\text{Fe}/\text{H}] = -0.57 \pm 0.20$ dex, and distance modulus $(m - M)_0 = 14.44 \pm 0.17$.

- We determined the center of Berkeley 76 - $\alpha_{J2000} = 07^h06^m42.4^s$ and $\delta_{J2000} = -11^\circ43'33''$. For the physical quantities: we obtained radius $4.0' \pm 0.3'$, color excess $E(B - V) = 0.41 \pm 0.33$, age $t = 1.26 \pm 0.14$ Gyr ($\log t = 9.10 \pm 0.05$), metallicity $[\text{Fe}/\text{H}] = 0.00 \pm 0.20$ dex, and distance modulus $(m - M)_0 = 13.97 \pm 0.23$.
- We investigated the radial metallicity distribution of the Galactic disk using a single linear fit and a broken linear fit to 236 old OCs. The gradient of the single linear fit was -0.052 ± 0.004 dex kpc⁻¹, and those for the broken linear fit were -0.070 ± 0.006 dex kpc⁻¹ at $r < 12$ kpc and -0.016 ± 0.010 at $r \geq 12$ kpc.

Software: Scipy (Jones et al. 2001), astrometry.net (Lang et al. 2010), IRAF (Tody 1986, 1993), DAOPHOT II/ALLSTAR (Stetson 1990), PARSEC (Bressan et al. 2012), pyUPMASK (Pera et al. 2021).

ACKNOWLEDGMENTS

We thank the anonymous referee for the fast and very helpful comments that improved the manuscript. We thank A. E. Piatti for sending us the photometric data of Czernik 30 and Takashi Hasegawa for providing us the photometric data of Berkeley 76. We appreciate Mridweeka Singh for helpful discussion. Based on observations at Cerro Tololo Inter-American Observatory at NSF's NOIRLab (NOIRLab Prop. ID 2010B-0178; PI: Sang Chul Kim), which is managed by the Association of Universities for Research in Astronomy (AURA) under a cooperative agreement with the National Science Foundation. This publication makes use of data products from the Two Micron All Sky Survey, which is a joint project of the University of Massachusetts and the Infrared Processing and Analysis Center/California Institute of Technology, funded by the National Aeronautics and Space Administration and the National Science Foundation. This work has made use of data from the European Space Agency (ESA) mission *Gaia* (<https://www.cosmos.esa.int/gaia>), processed by the *Gaia* Data Processing and Analysis Consortium (DPAC, <https://www.cosmos.esa.int/web/gaia/dpac/consortium>). Funding for the DPAC has been provided by national institutions, in particular the institutions participating in the *Gaia* Multilateral Agreement. This research was supported by the Korea Astronomy and Space Science Institute under the R&D program (Project No. 2022-1-868-04) supervised by the Ministry of Science and ICT. H.S.P. was supported in part by the National Research Foundation of Korea (NRF) grant funded by the Korea government (MSIT, Ministry of Science and ICT; No. NRF-2019R1F1A1058228). J.H.L. was supported by the National Research Foundation of Korea (NRF) grant funded by the Korea government (MSIT) (No. 2022R1A2C1004025).

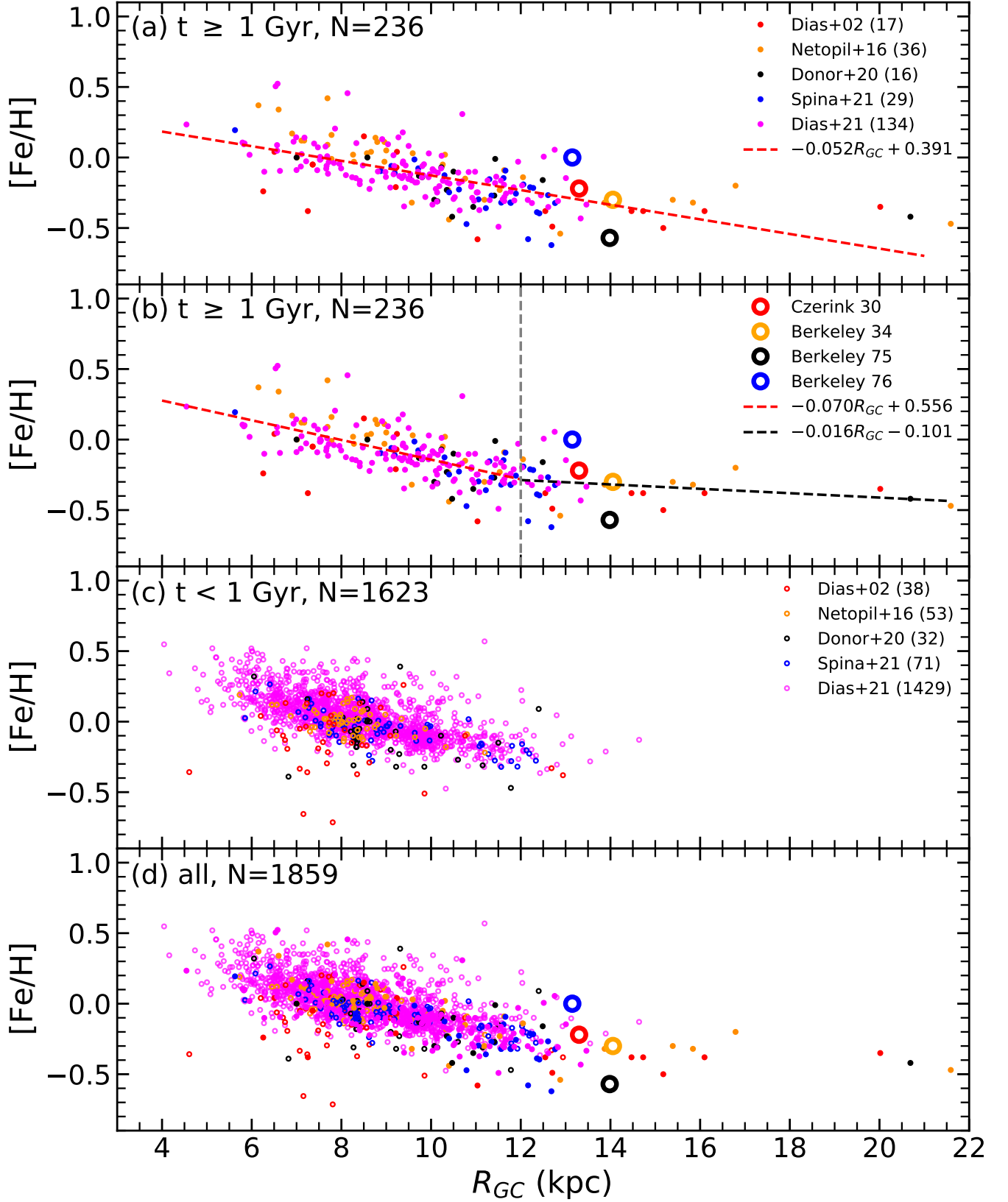


Figure 15. Radial metallicity distribution in the Galactic disk. (a) is the result of single linear fitting to old OCs. (b) shows the broken linear fit result with the discontinuity at 12 kpc. (c) is the distribution of OCs younger than 1 Gyr. (d) is the radial metallicity distribution for the OCs in all age ranges.

REFERENCES

- Ahumada, A. V., Cignoni, M., Bragaglia, A., et al. 2013, *MNRAS*, 430, 221, doi: [10.1093/mnras/sts593](https://doi.org/10.1093/mnras/sts593)
- Alves, D. R. 2000, *ApJ*, 539, 732, doi: [10.1086/309278](https://doi.org/10.1086/309278)
- Bessell, M. S. 2001, *PASP*, 113, 66, doi: [10.1086/317972](https://doi.org/10.1086/317972)
- Bressan, A., Marigo, P., Girardi, L., et al. 2012, *MNRAS*, 427, 127, doi: [10.1111/j.1365-2966.2012.21948.x](https://doi.org/10.1111/j.1365-2966.2012.21948.x)
- Cannon, R. D. 1970, *MNRAS*, 150, 111, doi: [10.1093/mnras/150.1.111](https://doi.org/10.1093/mnras/150.1.111)
- Cantat-Gaudin, T., Donati, P., Vallenari, A., et al. 2016, *A&A*, 588, A120, doi: [10.1051/0004-6361/201628115](https://doi.org/10.1051/0004-6361/201628115)
- Cantat-Gaudin, T., Jordi, C., Vallenari, A., et al. 2018a, *A&A*, 618, A93, doi: [10.1051/0004-6361/201833476](https://doi.org/10.1051/0004-6361/201833476)
- Cantat-Gaudin, T., Vallenari, A., Sordo, R., et al. 2018b, *A&A*, 615, A49, doi: [10.1051/0004-6361/201731251](https://doi.org/10.1051/0004-6361/201731251)
- Cantat-Gaudin, T., Anders, F., Castro-Ginard, A., et al. 2020, *A&A*, 640, A1, doi: [10.1051/0004-6361/202038192](https://doi.org/10.1051/0004-6361/202038192)
- Carraro, G., Beletsky, Y., & Marconi, G. 2013, *MNRAS*, 428, 502, doi: [10.1093/mnras/sts038](https://doi.org/10.1093/mnras/sts038)
- Carraro, G., Geisler, D., Moitinho, A., Baume, G., & Vázquez, R. A. 2005, *A&A*, 442, 917, doi: [10.1051/0004-6361:20053089](https://doi.org/10.1051/0004-6361:20053089)
- Carraro, G., Geisler, D., Villanova, S., Frinchaboy, P. M., & Majewski, S. R. 2007, *A&A*, 476, 217, doi: [10.1051/0004-6361:20078113](https://doi.org/10.1051/0004-6361:20078113)
- Carrera, R., Rodríguez Espinosa, L., Casamiquela, L., et al. 2017, *MNRAS*, 470, 4285, doi: [10.1093/mnras/stx1526](https://doi.org/10.1093/mnras/stx1526)
- Carrera, R., Pasquato, M., Vallenari, A., et al. 2019, *A&A*, 627, A119, doi: [10.1051/0004-6361/201935599](https://doi.org/10.1051/0004-6361/201935599)
- Chan, V. C., & Bovy, J. 2020, *MNRAS*, 493, 4367, doi: [10.1093/mnras/staa571](https://doi.org/10.1093/mnras/staa571)
- Chen, Y. Q., Casagrande, L., Zhao, G., et al. 2017, *ApJ*, 840, 77, doi: [10.3847/1538-4357/aa6d0f](https://doi.org/10.3847/1538-4357/aa6d0f)
- Chen, Y. Q., & Zhao, G. 2020, *MNRAS*, 495, 2673, doi: [10.1093/mnras/staa1079](https://doi.org/10.1093/mnras/staa1079)
- Dias, W. S., Alessi, B. S., Moitinho, A., & Lépine, J. R. D. 2002, *A&A*, 389, 871, doi: [10.1051/0004-6361:20020668](https://doi.org/10.1051/0004-6361:20020668)
- Dias, W. S., Monteiro, H., Moitinho, A., et al. 2021, *MNRAS*, 504, 356, doi: [10.1093/mnras/stab770](https://doi.org/10.1093/mnras/stab770)
- Donati, P., Bragaglia, A., Cignoni, M., Coccozza, G., & Tosi, M. 2012, *MNRAS*, 424, 1132, doi: [10.1111/j.1365-2966.2012.21289.x](https://doi.org/10.1111/j.1365-2966.2012.21289.x)
- Donor, J., Frinchaboy, P. M., Cunha, K., et al. 2020, *AJ*, 159, 199, doi: [10.3847/1538-3881/ab77bc](https://doi.org/10.3847/1538-3881/ab77bc)
- Francis, C., & Anderson, E. 2014, *MNRAS*, 441, 1105, doi: [10.1093/mnras/stu631](https://doi.org/10.1093/mnras/stu631)
- Friel, E. D. 1995, *ARA&A*, 33, 381, doi: [10.1146/annurev.aa.33.090195.002121](https://doi.org/10.1146/annurev.aa.33.090195.002121)
- Gaia Collaboration, Antoja, T., McMillan, P. J., et al. 2021, *A&A*, 649, A8, doi: [10.1051/0004-6361/202039714](https://doi.org/10.1051/0004-6361/202039714)
- Girardi, L. 2016, *ARA&A*, 54, 95, doi: [10.1146/annurev-astro-081915-023354](https://doi.org/10.1146/annurev-astro-081915-023354)
- Grocholski, A. J., & Sarajedini, A. 2002, *AJ*, 123, 1603, doi: [10.1086/339027](https://doi.org/10.1086/339027)
- Groenewegen, M. A. T. 2008, *A&A*, 488, 935, doi: [10.1051/0004-6361:200810201](https://doi.org/10.1051/0004-6361:200810201)
- Hasegawa, T., Malasan, H. L., Kawakita, H., et al. 2004, *PASJ*, 56, 295, doi: [10.1093/pasj/56.2.295](https://doi.org/10.1093/pasj/56.2.295)
- Hasegawa, T., Sakamoto, T., & Malasan, H. L. 2008, *PASJ*, 60, 1267, doi: [10.1093/pasj/60.6.1267](https://doi.org/10.1093/pasj/60.6.1267)
- Hawkins, K., Leistedt, B., Bovy, J., & Hogg, D. W. 2017, *MNRAS*, 471, 722, doi: [10.1093/mnras/stx1655](https://doi.org/10.1093/mnras/stx1655)
- Hayes, C. R., Friel, E. D., Slack, T. J., & Boberg, O. M. 2015, *AJ*, 150, 200, doi: [10.1088/0004-6256/150/6/200](https://doi.org/10.1088/0004-6256/150/6/200)
- Janes, K. A. 1979, *ApJS*, 39, 135, doi: [10.1086/190568](https://doi.org/10.1086/190568)
- Janes, K. A., & Phelps, R. L. 1994, *AJ*, 108, 1773, doi: [10.1086/117192](https://doi.org/10.1086/117192)
- Jones, E., Oliphant, T., & Peterson, P. 2001, *SciPy: Open Source Scientific Tools for Python*. <http://www.scipy.org>
- Kharchenko, N. V., Piskunov, A. E., Schilbach, E., Röser, S., & Scholz, R. D. 2013, *A&A*, 558, A53, doi: [10.1051/0004-6361/201322302](https://doi.org/10.1051/0004-6361/201322302)
- Kim, S. C. 2006, *Journal of Korean Astronomical Society*, 39, 115, doi: [10.5303/JKAS.2006.39.4.115](https://doi.org/10.5303/JKAS.2006.39.4.115)
- Kim, S. C., Kyeong, J., Park, H. S., et al. 2017, *Journal of Korean Astronomical Society*, 50, 79, doi: [10.5303/JKAS.2017.50.3.79](https://doi.org/10.5303/JKAS.2017.50.3.79)
- Kim, S. C., Kyeong, J., & Sung, E.-C. 2009, *Journal of Korean Astronomical Society*, 42, 135, doi: [10.5303/JKAS.2009.42.6.135](https://doi.org/10.5303/JKAS.2009.42.6.135)
- Kim, S. C., & Sung, H. 2003, *Journal of Korean Astronomical Society*, 36, 13, doi: [10.5303/JKAS.2003.36.1.013](https://doi.org/10.5303/JKAS.2003.36.1.013)
- Krone-Martins, A., & Moitinho, A. 2014, *A&A*, 561, A57, doi: [10.1051/0004-6361/201321143](https://doi.org/10.1051/0004-6361/201321143)
- Kyeong, J., Kim, S. C., Hiriart, D., & Sung, E.-C. 2008, *Journal of Korean Astronomical Society*, 41, 147, doi: [10.5303/JKAS.2008.41.6.147](https://doi.org/10.5303/JKAS.2008.41.6.147)
- Kyeong, J., Moon, H.-K., Kim, S. C., & Sung, E.-C. 2011, *Journal of Korean Astronomical Society*, 44, 33, doi: [10.5303/JKAS.2011.44.1.033](https://doi.org/10.5303/JKAS.2011.44.1.033)
- Kyeong, J.-M., Byun, Y.-I., & Sung, E.-C. 2001, *Journal of Korean Astronomical Society*, 34, 143, doi: [10.5303/JKAS.2001.34.3.143](https://doi.org/10.5303/JKAS.2001.34.3.143)

² the BIC statistic is a method for scoring and selecting a model, and the model with the lowest BIC is selected.

- Lada, C. J., & Lada, E. A. 2003, *ARA&A*, 41, 57, doi: [10.1146/annurev.astro.41.011802.094844](https://doi.org/10.1146/annurev.astro.41.011802.094844)
- Landolt, A. U. 1992, *AJ*, 104, 340, doi: [10.1086/116242](https://doi.org/10.1086/116242)
- . 2009, *AJ*, 137, 4186, doi: [10.1088/0004-6256/137/5/4186](https://doi.org/10.1088/0004-6256/137/5/4186)
- Landolt, A. U., & Uomoto, A. K. 2007, *AJ*, 133, 768, doi: [10.1086/510485](https://doi.org/10.1086/510485)
- Laney, C. D., Joner, M. D., & Pietrzyński, G. 2012, *MNRAS*, 419, 1637, doi: [10.1111/j.1365-2966.2011.19826.x](https://doi.org/10.1111/j.1365-2966.2011.19826.x)
- Lang, D., Hogg, D. W., Mierle, K., Blanton, M., & Roweis, S. 2010, *AJ*, 139, 1782, doi: [10.1088/0004-6256/139/5/1782](https://doi.org/10.1088/0004-6256/139/5/1782)
- Liu, L., & Pang, X. 2019, *ApJS*, 245, 32, doi: [10.3847/1538-4365/ab530a](https://doi.org/10.3847/1538-4365/ab530a)
- Lyngå, G. 1995, *VizieR Online Data Catalog*, VII/92A
- Minchev, I., Chiappini, C., & Martig, M. 2013, *A&A*, 558, A9, doi: [10.1051/0004-6361/201220189](https://doi.org/10.1051/0004-6361/201220189)
- Minchev, I., Anders, F., Recio-Blanco, A., et al. 2018, *MNRAS*, 481, 1645, doi: [10.1093/mnras/sty2033](https://doi.org/10.1093/mnras/sty2033)
- Monteiro, H., Barros, D. A., Dias, W. S., & Lépine, J. R. D. 2021, *Frontiers in Astronomy and Space Sciences*, 8, 62, doi: [10.3389/fspas.2021.656474](https://doi.org/10.3389/fspas.2021.656474)
- Netopil, M., Oralhan, İ. A., Çakmak, H., Michel, R., & Karataş, Y. 2022, *MNRAS*, 509, 421, doi: [10.1093/mnras/stab2961](https://doi.org/10.1093/mnras/stab2961)
- Netopil, M., Paunzen, E., Heiter, U., & Soubiran, C. 2016, *A&A*, 585, A150, doi: [10.1051/0004-6361/201526370](https://doi.org/10.1051/0004-6361/201526370)
- Nishiyama, S., Tamura, M., Hatano, H., et al. 2009, *ApJ*, 696, 1407, doi: [10.1088/0004-637X/696/2/1407](https://doi.org/10.1088/0004-637X/696/2/1407)
- Ortolani, S., Bica, E., Barbuy, B., & Zoccali, M. 2005, *A&A*, 439, 1135, doi: [10.1051/0004-6361:20041458e](https://doi.org/10.1051/0004-6361:20041458e)
- Park, H. S., & Lee, M. G. 1999, *MNRAS*, 304, 883, doi: [10.1046/j.1365-8711.1999.02366.x](https://doi.org/10.1046/j.1365-8711.1999.02366.x)
- Pera, M. S., Perren, G. I., Moitinho, A., Navone, H. D., & Vazquez, R. A. 2021, *A&A*, 650, A109, doi: [10.1051/0004-6361/202040252](https://doi.org/10.1051/0004-6361/202040252)
- Perren, G. I., Vázquez, R. A., & Piatti, A. E. 2015, *A&A*, 576, A6, doi: [10.1051/0004-6361/201424946](https://doi.org/10.1051/0004-6361/201424946)
- Phelps, R. L., Janes, K. A., & Montgomery, K. A. 1994, *AJ*, 107, 1079, doi: [10.1086/116920](https://doi.org/10.1086/116920)
- Piatti, A. E., Clariá, J. J., Parisi, M. C., & Ahumada, A. V. 2009, *NewA*, 14, 97, doi: [10.1016/j.newast.2008.05.006](https://doi.org/10.1016/j.newast.2008.05.006)
- Ruiz-Dern, L., Babusiaux, C., Arenou, F., Turon, C., & Lallement, R. 2018, *A&A*, 609, A116, doi: [10.1051/0004-6361/201731572](https://doi.org/10.1051/0004-6361/201731572)
- Sim, G., Lee, S. H., Ann, H. B., & Kim, S. 2019, *Journal of Korean Astronomical Society*, 52, 145, doi: [10.5303/JKAS.2019.52.5.145](https://doi.org/10.5303/JKAS.2019.52.5.145)
- Skrutskie, M. F., Cutri, R. M., Stiening, R., et al. 2006, *AJ*, 131, 1163, doi: [10.1086/498708](https://doi.org/10.1086/498708)
- Spina, L., Magrini, L., & Cunha, K. 2022, *Universe*, 8, 87, doi: [10.3390/universe8020087](https://doi.org/10.3390/universe8020087)
- Spina, L., Ting, Y. S., De Silva, G. M., et al. 2021, *MNRAS*, 503, 3279, doi: [10.1093/mnras/stab471](https://doi.org/10.1093/mnras/stab471)
- Stetson, P. B. 1990, *PASP*, 102, 932, doi: [10.1086/132719](https://doi.org/10.1086/132719)
- Tadross, A. L. 2008, *MNRAS*, 389, 285, doi: [10.1111/j.1365-2966.2008.13554.x](https://doi.org/10.1111/j.1365-2966.2008.13554.x)
- Tody, D. 1986, in *Society of Photo-Optical Instrumentation Engineers (SPIE) Conference Series*, Vol. 627, *Instrumentation in astronomy VI*, ed. D. L. Crawford, 733, doi: [10.1117/12.968154](https://doi.org/10.1117/12.968154)
- Tody, D. 1993, in *Astronomical Society of the Pacific Conference Series*, Vol. 52, *Astronomical Data Analysis Software and Systems II*, ed. R. J. Hanisch, R. J. V. Brissenden, & J. Barnes, 173
- Twarog, B. A., Ashman, K. M., & Anthony-Twarog, B. J. 1997, *AJ*, 114, 2556, doi: [10.1086/118667](https://doi.org/10.1086/118667)
- van den Bergh, S., & McClure, R. D. 1980, *A&A*, 88, 360
- van Helshoecht, V., & Groenewegen, M. A. T. 2007, *A&A*, 463, 559, doi: [10.1051/0004-6361:20052721](https://doi.org/10.1051/0004-6361:20052721)
- Wang, S., & Chen, X. 2021, *ApJ*, in print, arXiv:2108.13605. <https://arxiv.org/abs/2108.13605>
- Zhang, H., Chen, Y., & Zhao, G. 2021, *ApJ*, 919, 52, doi: [10.3847/1538-4357/ac0e92](https://doi.org/10.3847/1538-4357/ac0e92)
- Zhong, J., Chen, L., Jiang, Y., Qin, S., & Hou, J. 2022, *AJ*, 164, 54, doi: [10.3847/1538-3881/ac77fa](https://doi.org/10.3847/1538-3881/ac77fa)